ANALYSIS OF THE RESULTS OF THE OEEPE TEST "INTEGRATED SENSOR ORIENTATION"

Christian Heipke, Karsten Jacobsen, Helge Wegmann, Hannover

ABSTRACT

The European Organisation for Experimental Photogrammetric Research (OEEPE) has embarked on a multi-site test investigating sensor orientation using GPS and IMU in comparison and in combination with aerial triangulation. The test was expected to demonstrate the extent to which direct and integrated sensor orientation are accurate and efficient methods for the determination of the exterior orientation parameters for large scale topographic mapping. Another test goal was the transfer of the recently developed technology from the research arena to potential users.

In this paper we describe the test results. In direct sensor orientation RMS differences for point determination of 5 – 10 cm in planimetry and 10 – 15 cm in height at independent check points have been obtained for multi-ray points at an image scale 1:5 000. For two-ray points the RMS differences are higher by only a factor of about 1.5. While these values are larger by a factor of 2 – 3 when compared to standard photogrammetric results, it seems to be safe to conclude that direct sensor orientation currently allows for the generation of orthoimages and point determination with less stringent accuracy requirements. Reports from practical applications demonstrate a significant decrease in time and thus cost for direct sensor orientation compared to conventional and GPS-photogrammetry. Stereo plotting, on the other hand, is not always possible using direct sensor orientation due to the sometimes large y-parallaxes in individual models.

Compared to direct sensor orientation, the additional introduction of tie points in integrated sensor orientation without GCPs improves in particular the accuracy in image space, and to some extent also in object space. Thus, as was to be expected, integrated sensor orientation overcomes the problem of remaining y-parallaxes in photogrammetric models and allows for the determination of 3D object space information in much the same way as conventional photogrammetry.

The reliability of the results remains a weak point of direct and integrated sensor orientation due to a lack of redundancy in absolute orientation. Systematic errors in the GPS/IMU measurements or changes in the system calibration parameters between calibration and actual flight may go unnoticed, because they cannot be detected without the introduction of GCP coordinates. Thus, it is recommended to include at least a minimum number of GCPs in the actual project area wherever possible.

In summary, it is expected that direct sensor orientation will be the dominating technology for sensor orientation. Of particular relevance is a properly carried out system calibration. Integrated sensor orientation will be applied whenever very high accuracy is indispensable, and thus tie points are needed in order to model effects in image space using additional parameters. Future developments in GPS and IMU sensor technology and data processing will probably further improve the potential of direct and integrated sensor orientation.

1 DATA PREPARATION

Once the test flights had taken place the preparation of the test data started. It consisted of GPS/ IMU pre-processing, a check of the computed data by comparing the results derived from different reference stations, and the manual measurement of image coordinates in all acquired images.

1.1 GPS/IMU pre-processing and checking

Details of GPS/IMU pre-processing were considered proprietary information by Applanix and IGI. Consequently, within the arrangements made for the test, pre-processing was carried out by the two companies. Pre-processing consisted of the transformation of the raw GPS and IMU measurements

into object space coordinates for the camera projection centres, and roll, pitch and yaw values for each image. It was decided to use the EUREF89/UTM system, zone 32 with ellipsoidal heights, as object space coordinate system in the test (thus compatibility with the object space coordinates of the test field was maintained), and the GPS positions for the camera projection centres had to be computed in this system. Since the position information refers to the projection centres, the lever arm corrections describing the difference in position between the GPS antenna, the IMU coordinate origin and the origin of the camera coordinate system (more precisely, the entrance node of the camera lens) had to be taken into account during pre-processing. Roll, pitch and yaw values had to conform to the ARINC 705 convention (ARINC 2001), describing a three-dimensional rotation from local level coordinate system to the body frame of the aircraft. It should be noted, that two assumptions were introduced into the pre-processing step: The alignment of the EUREF89 and the WGS84 coordinate systems is assumed to be identical, and no geoid information was introduced. Thus the local Z-axis was assumed to be parallel to the local gravity vector (the deflection of the vertical was assumed to be zero).
Five different reference stations were used to compute the GPS/IMU values for each flight. A first check based only on GPS data and carried out by the pilot centre showed that the aircraft trajectories computed from the different reference stations all agreed very well (Leistner 2000). In a second step Applanix and IGI computed trajectories and roll, pitch, yaw values for the aircraft, again for all five reference stations and reported that also these results agreed very well. In order to separate effects stemming from long GPS base lines from those of sensor orientation, the data of the reference station "Fredrikstad" located in the middle of the IKF test field itself were finally chosen for the test. While one of the companies had subsampled the high frequency GPS/IMU data and delivered the GPS positions of the camera projection centres and the roll, pitch and yaw values for each instant of exposure to the pilot centre, the other one delivered the high frequency data itself. Unfortunately, no statistical information about the accuracy of the data was available from either company. In order to provide identical conditions for the test, only the GPS/IMU data for the instant of image exposure were used in the further processing. Plots showed that these data were generally free of errors, although some heading values were clearly wrong.

1.2 Reference measurements in the images

In order to check the acquired images the pilot centre manually measured image coordinates of all points of the test field and a large number of tie points in each of the calibration and test flight images using an analytical plotter, and subsequently performed a conventional bundle adjustment. The results of the bundle adjustment are presented in table 1 containing the root mean square (RMS) differences of the adjustment calculated over a number of independent check points. The bundle adjustment was computed including twelve parameters for self calibration. These parameters, however, had very little effect on the results. In table 1 and the remainder of this paper Company_1 represents the FW/IGI data set, and Company_2 the Fotonor/Applanix data set. These aliases have been introduced in order to separate the test participants Applanix and IGI (see below) from the data sets provided by these companies.

Table 1: Results of aerial triangulation performed for the calibration flights

		No. of images	**No. of control points**		**No. of check points**		σ_0	**RMS X**	**RMS_ Y**	**RMS Z**
			planimetry	height	planimetry	height	[µm]	[cm]	[cm]	[cm]
IGI (Company_1)	Calibration 1:5 000	62	12	12	12	11	4.4	2.8	2.0	3.2
	Calibration 1:10 000	86	13	13	36	35	4.1	2.6	3.0	5.7
	Test flight	117	13	13	28	27	4.8	2.8	2.6	4.3
Applanix (Company_2)	Calibration 1:5 000	66	12	12	12	11	5.1	1.8	1.2	8.0
	Calibration 1:10 000	85	13	13	36	35	4.8	2.9	3.0	7.9
	Test flight	181	13	13	36	36	5.6	2.2	2.0	6.0

The obtained results demonstrate that the images and the measurements can be used in the test. It should be noted that the calibration flight 1:5 000 consists of two strips in perpendicular direction, both flown twice only (thus exhibiting a rather weak geometry), which explains that the RMS differences on the ground are in the same range as those for the 1:10 000 calibration flight. The standard deviations of the image coordinates differ a little between the two companies, probably due to the somewhat poorer image quality of Company_2.

2 TEST PARTICIPANTS

All test data as described in Heipke et al. (2002) were sent out to the test participants[1]. Thirty four potential test participants asked for the data. Twelve participants returned their results (refer to table 2[2]). As can be seen, besides the two companies having provided the GPS/IMU sensor systems, three software developers (GIP, inpho, LH Systems), one National Mapping Agency (ICC), one commercial user (ADR) and five research institutes (DIIAR, FGI, IPF, IPI and ifp) took part in the test. Thus, with the exception of the University of Calgary, which carried out much of the pioneering work in direct sensor orientation (Schwarz 1993; 1995), most parties currently active in this area are represented in the test. Nearly all participants used existing bundle adjustment programmes, partly augmented by additional software development. In this way, besides demonstrating the state-of-the-art in integrated sensor orientation, the distributed data also served as test data for refinements of the existing software, which is well within the goal of technology transfer[3].

Table 2: List of test participants (note that the same software name does not necessarily imply the same version and thus the same results)

Test participant	Abbreviation	Participated in phase	Software used
Applanix, Canada	Applanix	I	POS tools
IGI, Germany	IGI	I	AEROoffice tools and BINGO
ADR, BAE Systems, USA	ADR	I	BLUH
Finnish Geodetic Institute, Masala	FGI	I and II	own development, called FGIAT
GIP, Germany	GIP	I	BINGO
ICC Barcelona, Spain	ICC	I and II	GeoTex/ACX
inpho, Germany	Inpho	I and II	inBlock
LH Systems, USA	LHS	(I) and II	ORIMA
Politecnico di Milano, Italy	DIIAR	I and II	own development
Technical University Vienna, Austria	IPF	I and II	ORIENT
University of Hannover, Germany	IPI	I and II	BLUH
University of Stuttgart, Germany	Ifp	I and II	PAT B and own development

[1] The GPS/IMU data from IGI sent out at first contained an error due to an inappropriate consideration of the initial alignment process during GPS/IMU pre-processing. This error was detected by IGI shortly afterwards, and corrected GPS/IMU data were subsequently distributed to the participants. The results presented in this paper refer exclusively to the second data set. The first incorrect data set is not further considered.

[2] In phase I LHS only processed the Company_1 data set. After the deadline for returning the results to the pilot centre and in preparation for phase II, the Company_2 data were also processed. Therefore, LHS could take part in phase II with Company_1 and Company_2 results.

[3] This fact explains that some of the results reported in this paper slightly differ from results published earlier. During the test the pilot centre was continuously in contact with all participants and over time received various results from some of them. The tables contained in this paper constitute the final test results.

3 PHASE I: DIRECT SENSOR ORIENTATION

As is described in Heipke et al. (2002) data delivered to the participants in phase I of the test included the pre-processed GPS/IMU data for the calibration flights and the test flight together with the object space coordinates of some GCPs and their image coordinates from the calibration flights. The task was to carry out a system calibration based on the calibration flight data followed by the determination of the exterior orientation parameters of the test flight. These results were to be sent back to the pilot centre. Subsequently a least-squares forward intersection was performed using the computed exterior orientation as constant values and image coordinates of check points measured in the test flight images by the pilot centre.

The analysis of the differences of the 3D coordinates of the forward intersection and the known independent check point (ICP) coordinates on the ground as well as the corresponding residuals in image space is presented in this chapter. While it is obvious that in object space a comparison between the computed coordinates and those of independent check points can serve to judge the results, it is not clear a priori how to assess the derived orientation parameters themselves. Rather than trying to analyse the GPS/IMU measurements and the parameters of exterior orientation computed by the participants, and to quantify their accuracy, we have taken a users´ perspective for this test and have looked at remaining y-parallaxes in the resulting stereo models. The reason for this approach was that the most sensitive application for the image orientations in terms of accuracy is that of stereo plotting, which relies on models free of y-parallaxes.

3.1 System calibration approaches

The results delivered to the pilot centre have been analysed and are presented in this chapter. As was to be expected the individual participants have used different approaches for computing the system calibration parameters. A description of the standard approach can be found e.g. in Skaloud (1999; Cramer 2001), and it will not be repeated here. Although the exact procedures adopted by the participants were not always released in detail, a number of noticeable distinctions could be observed (see also table 3 and 4):

- Mathematical model for system calibration: The exact mathematical model used and the number of system calibration parameters estimated in the adjustment differed across the various solutions. Many participants used the six standard parameters (three GPS shifts, three misalignment angles), which can be computed from only one calibration flight. Some participants also corrected for the parameters of interior orientation and the additional parameters known from camera self-calibration. DIIAR also investigated the time synchronisation between the attitude values and the exposure time by estimating a constant time shift (Skaloud 1999), but found that based on the distributed data no correction needed to be applied (Forlani, Pinto 2002). In table 3 these approaches are grouped into three categories: standard parameters (six unknowns), standard parameters and interior orientation (nine unknowns), and more refined approaches (more than nine unknowns). More details are contained in table 4 which contains the exact unknowns used by each participant.
- Determination of the system calibration parameters in a combined bundle adjustment run with the image coordinates of the calibration flights, the GPS/IMU data and the GCP object coordinates as input (denoted as “1 step” in table 3) vs. a comparison of the exterior orientation derived from a conventional bundle adjustment and the GPS/IMU values (“2 steps”): In the latter approach some participants averaged the differences of the photogrammetric and the GPS/IMU results to compute the calibration parameters, disregarding the correlations between the different parameter groups. Others used a more sophisticated computational scheme. DIIAR, for example, weighted the influence of the photogrammetrically determined exterior orientation parameters based on the corresponding theoretical standard deviations derived from the bundle adjustment (Forlani, Pinto 2002).
- UTM vs. local tangential coordinate system: Most participants carried out all computations in the UTM system; LHS transformed the input data into a local tangential system, computed the results, and subsequently transformed them into the UTM system (denoted by * in table 3); DIIAR and ifp processed and delivered results in the local tangential system, IPI processed and delivered re-

sults in both systems (see Jacobsen 2002 for effects of using a curvilinear coordinate system such as UTM in direct and integrated sensor orientation).

– Input information used: This information must be seen in conjunction with the number of unknown parameters of the mathematical model. Some participants used the image coordinates of both calibration flights in one simultaneous adjustment, others performed separate adjustments and subsequently combined the results, while yet others used one calibration flight only. In some cases, the GPS shifts were determined from only one flight while the boresight misalignment was derived from both. Some participants also deleted the first and the last few images from the computations, arguing that the corresponding data were not suited for the calibration.

Table 3: Overview of system calibration approaches used by the different participants

Participant	**Number of system calibration parameters**		**Procedure**	**Object space coord. system used for the computations**
	Company_1	Company_2		
Applanix	-	6	1 step	UTM
IGI	6	-	1 step	UTM
ADR	6	6	2 steps	UTM
FGI	> 9	> 9	2 steps	UTM
GIP	> 9	> 9	1 step	UTM
ICC	> 9	> 9	1 step	UTM
inpho	6	9	1 step	UTM
LHS	6	-	1 step	Local tangential*
DIIAR	6	6	2 steps	Local tangential
IPF	> 9	> 9	1 step	UTM
IPI	> 9	> 9	2 steps	Local tangential and UTM
ifp	5	6	2 steps	Local tangential

Table 4: Unknowns within the system calibration model for each participant
drpy denotes roll, pitch and yaw (boresight misalignment) dXoYoZo denotes GPS shift parameters in the three object space coordinates dcxpyp denotes the parameters of interior orientation

Participant	**Number of system calibration parameters**		**Used system calibration parameters**	
	Company_1	Company_2	Company_1	Company_2
Applanix	-	6	-	drpy + dXoYoZo
IGI	6	-	drpy + dXoYoZo	-
ADR	6	6	drpy + dXoYoZo	drpy + dXoYoZo
FGI	18	19	drpy + dXoYoZo + 12 add. par.	drpy + dXoYoZo + dc + 12 add. par.
GIP	12	12	drpy + dXoYoZo + dcxpyp + 3 add. par.	drpy + dXoYoZo + dcxpyp + 3 add. par.
ICC	21	21	drpy + dXoYoZo + dcxpyp + 12 add. par.	drpy + dXoYoZo + dcxpyp + 12 add. par.
inpho	6	9	drpy + dXoYoZo	drpy + dXoYoZo + dcxpyp
LHS	6	-	drpy + dXoYoZo	-
DIIAR	6	6	drpy + dXoYoZo	drpy + dXoYoZo
IPF	11	11	drpy + dXoYoZo + dcxpyp + 2 add. par.	drpy + dXoYoZo + dcxpyp + 2 add. par.
IPI	21	21	drpy + dXoYoZo + dcxpyp + 12 add. par.	drpy + dXoYoZo + dcxpyp + 12 add. par.
ifp	5	6	drpy + dYo + dc	drpy + dcxpyp

It should be noted that since no stochastic information was available for the GPS/IMU measurements other than the general values given in the data sheets of the companies, the participants were left guessing as to how accurate and how correlated these values actually were.

3.2 Global analysis, overall results

As mentioned before, we transformed the manually measured image coordinates of the ICP into object space via a least-squares forward intersection with the exterior orientation of the participants being introduced as constant values. The resulting object space coordinates were then compared to the known values of the ICP yielding RMS differences. The residuals in image space are accumulated in the σ_o value of the forward intersection and can be thought of as a measure for remaining y-parallaxes in stereo models formed using the participants' exterior orientation (see below for a more detailed discussion). Statistical results of this procedure are given in table 5. Table 6 contains the systematic errors, derived from a 3D translation of the computed point cloud with respect to the ICP coordinates, and the maximum errors for each participant.

The following results can be derived from tables 5 and 6:

- The accuracy potential of direct sensor orientation as determined from the best results lies at approximately 5 – 10 cm in planimetry and 10 – 15 cm in height when expressed as RMS differences at independent check points, and at 15 – 20 μm when expressed as σ_o values of the overdetermined forward intersection in image space.
- These values are larger by a factor of 2 – 3 when compared to standard photogrammetric results. The fact that the σ_o values are rather large suggests that stereo plotting in individual models is problematic and that the accuracy of the image coordinates (see table 1) was not fully exploited, because the parameters of exterior orientation were not accurate enough. Therefore, improvements can be expected by refining the exterior orientation (see also chapter 4).
- The systematic errors are very small for most participants and rarely exceed 10 cm in either planimetry or height.
- The maximum errors are in the range of 30 – 50 cm. Only very few participants reached larger values.
- When comparing results across the different participants some variations are visible. These variations show that some approaches still have potential for improvement. The ADR results, for example, were obtained using a somewhat experimental software version. It can also be seen that IGI and Applanix did not obtain the best results for their respective data sets. These findings suggest that a refinement of the calibration models and software will lead to improved results, especially for the height component. Based on the available information a more detailed analysis is not reasonable.
- The results do not significantly depend on the method of computing the boresight misalignment (one or two steps).
- For the Company_1 data the results do not depend on the chosen object space coordinate system (see the two IPI results). The situation is different, however, for the Company_2 data. Here, the RMS differences for planimetry and, in particular, for the height are better in the more rigorous local tangential system than in the UTM system.
- The Company_2 results have somewhat smaller RMS differences compared to the Company_1 results. While a conclusive explanation for these differences cannot be given, the used hardware (dry-tuned vs. fibre optics gyros) and the less favourable GPS conditions during the Company_1 flight (Nilsen Jr. 2002) are possible reasons.

3.3 Influence of the calibration model

In table 7 detailed results for three representative participants are shown. The number of system calibration parameters is varied under otherwise identical conditions in order to study its influence (the

three parameters of ifp denote the three angles of misalignment). In the Company_1 data a noticeable dependency on the chosen calibration model was not found (see however the improvements for the GIP results). On the other hand, the Company_2 results significantly depend on the number of parameters estimated during system calibration. Allowing for a change in the calibrated focal length and the position of the principal point improves the results especially in height. As was to be expected

Table 5: Results of least-squares forward intersection

Participant	**No. of system calibration parameters**		**Company_1 (41 XY_ICPs; 40 Z_ICPs)**				**Company_2 (49 XYZ_ICPs)**			
			σ_o	RMS differences at ICP			σ_o	RMS differences at ICP		
	Comp_ 1	Comp_ 2	[μm]	X [cm]	Y [cm]	Z [cm]	[μm]	X [cm]	Y [cm]	Z [cm]
Applanix	-	6	-	-	-	-	22.2	5.9	11.9	32.0
IGI	6	-	36.7	15.9	16.1	23.0	-	-	-	-
ADR	6	6	55.5	19.9	16.8	28.8	32.2	13.4	12.7	18.1
FGI	> 9	> 9	27.4	11.8	10.1	18.6	13.6	3.9	3.2	9.2
GIP	> 9	> 9	22.9	8.1	8.3	11.2	14.8	6.8	3.3	8.1
ICC	> 9	> 9	25.8	9.0	12.3	17.4	13.9	5.1	3.0	8.4
Inpho	6	9	27.0	10.3	9.8	14.6	14.8	4.7	3.3	8.2
LHS	6	-	44.6	13.8	13.1	17.9	-	-	-	-
DIIAR	6	6	22.9	8.8	11.8	13.5	12.4	3.9	2.5	8.4
IPF	> 9	> 9	24.6	8.5	8.9	12.4	19.5	7.0	3.3	12.0
IPI (tang.)	> 9	> 9	43.0	12.7	12.6	18.4	16.2	5.5	4.0	7.9
IPI (UTM)	> 9	> 9	42.8	12.9	15.7	18.7	16.1	8.5	3.3	12.3
ifp	5	6	35.1	15.1	15.2	21.7	14.5	5.3	3.3	6.9

Table 6: Results of least-squares forward intersection, illustrating systematic effects and maximum differences at independent check points (ICPs)

Parti-cipant	**Company_1 (41 XY_ICPs; 40 Z_ICPs)**						**Company_2 (49 XYZ_ICPs)**					
	System. diff. at ICP			Max. diff. at ICP			System. diff. at ICP			Max. diff. at ICP		
	Xsys [cm]	Ysys [cm]	Zsys [cm]	Xmax [cm]	Ymax [cm]	Zmax [cm]	Xsys [cm]	Ysys [cm]	Zsys [cm]	Xmax [cm]	Ymax [cm]	Zmax [cm]
Applanix	-	-	-	-	-	-	-2.5	-5.4	-31.2	-16.8	17.2	-65.4
IGI	3.1	-9.8	-7.0	-49.1	-40.1	-56.9	-	-	-			
ADR	-2.6	-7.5	8.5	-74.1	-40.4	56.2	-11.2	10.0	13.4	-33.5	28.2	49.7
FGI	1.6	-3.4	7.2	22.4	-29.2	41.8	-0.6	-0.1	6.1	-10.7	10.3	28.9
GIP	-2.9	-1.4	-3.2	-22.9	-21.1	-36.6	-5.6	1.0	5.0	-19.4	7.3	-23.3
ICC	3.5	-10.4	2.3	21.8	-36.7	38.5	-3.2	0.3	5.1	-15.9	6.6	24.8
inpho	0.0	-3.1	2.4	21.7	-28.5	33.3	-3.0	0.6	6.3	-16.0	7.4	25.0
LHS	0.5	-7.0	0.8	35.3	-36.8	44.5	-	-	-	-	-	-
DIIAR	3.9	-8.8	-5.1	25.5	-29.2	-39.5	-1.8	-0.7	5.8	-12.6	6.4	24.4
IPF	0.8	-2.0	0.5	22.3	-22.7	-39.3	-4.1	-0.2	6.4	-19.4	-8.0	34.4
IPI (tang.)	-1.5	-3.9	5.1	-32.4	-29.5	34.1	-2.3	2.2	5.3	-16.9	10.9	24.6
IPI (UTM)	5.6	-11.0	7.7	37.0	-36.8	34.4	-7.0	-0.2	10.9	-21.0	7.5	29.8
ifp	3.2	-8.4	0.3	-47.3	-36.1	68.2	-3.3	1.0	3.3	-15.3	9.1	24.9

a further refinement using self calibration parameters did not lead to significantly better results. An exception to these findings, however, is the result obtained by DIIAR, as they only used six system calibration parameters and still obtained excellent results (see table 5). This may have to do with the weighing scheme used when computing the system calibration parameters, however, no conclusive explanation is available for this result.
These findings are further confirmed by graphical analysis. To this end, first the RMS differences in object space were plotted in the XY plane. The plots of one participant (GIP) are presented in the figures 1 – 4. Figures 1 and 2 show the results for Company_1 and Company_2 achieved using six system calibration parameters (three GPS shifts and three misalignment angles), while figures 3 and 4 show the same information obtained from a system calibration with more than nine parameters.

Table 7: Detailed results for a varying number of calibration parameters, in the case of participants ifp, GIP and IPI

Participant	**No. of system calibration parameters**		**Company_1**				**Company_2**			
			σ_o	RMS differences at ICPs			σ_o	RMS differences at ICPs		
	Company_1	Company_2	[µm]	X [cm]	Y [cm]	Z [cm]	[µm]	X [cm]	Y [cm]	Z [cm]
ifp	3	3	35.5	14.9	15.6	25.0	31.3	11.1	8.7	15.1
	5	6	35.1	15.1	15.2	21.7	14.5	5.3	3.3	6.9
GIP	6	6	28.1	11.6	12.0	15.1	30.2	13.4	12.3	11.8
	> 9	> 9	22.9	8.1	8.3	11.2	14.8	10.7	11.2	8.1
IPI (tang.)	6	6	43.8	13.3	13.4	19.2	33.7	10.3	11.0	16.6
	9	9	43.0	12.7	12.6	18.4	17.1	6.1	3.8	8.0
	> 9	> 9	43.0	12.7	12.6	18.4	16.2	5.5	4.0	7.9

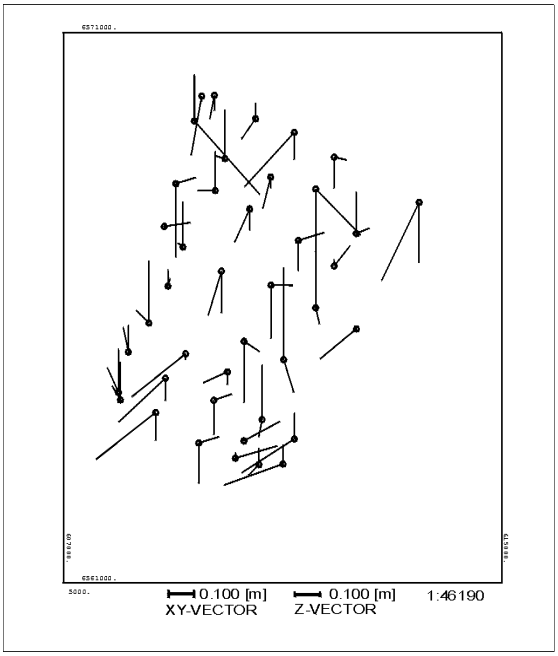

Figure 1: Difference vectors in planimetry and height, Company_1,
Participant GIP, six system calibration parameters

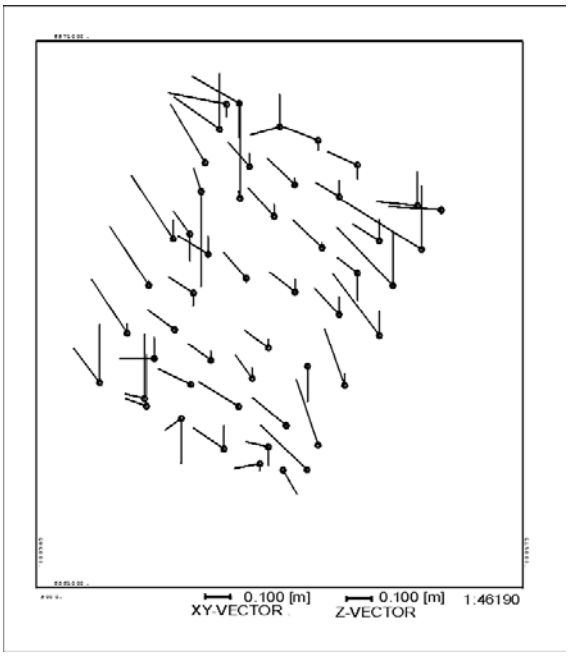

Figure 2: Difference vectors in planimetry and height, Company_2,
Participant GIP, six system calibration parameters

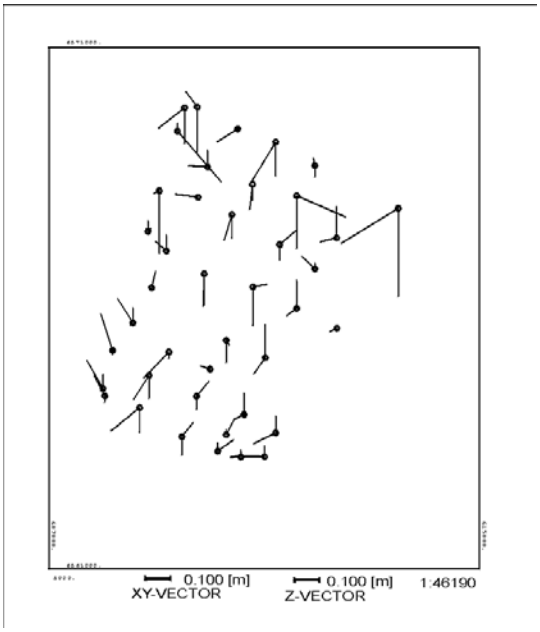

Figure 3: Difference vectors in planimetry and height, Company_1, Participant GIP, twelve system calibration parameters

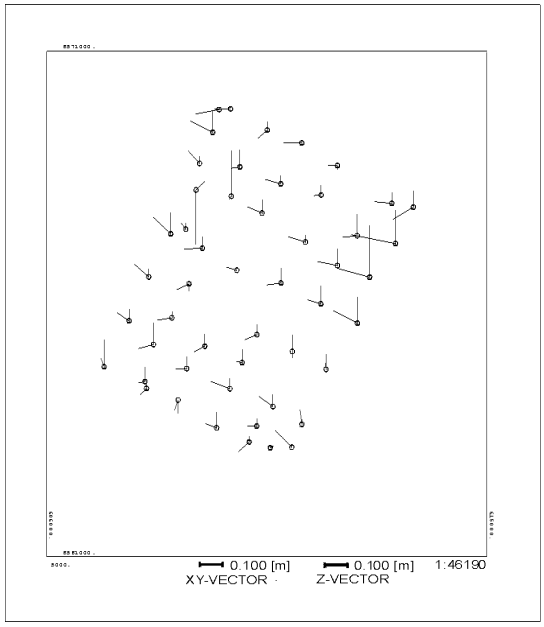

Figure 4: Difference vectors in planimetry and height, Company_2, Participant GIP, twelve system calibration parameters

In the Company_2 data set a systematic effect can clearly be seen in the six parameter solution, while it has vanished when using more than nine parameters. For the Company_1 results no such systematic effect is visible, although the RMS differences become somewhat smaller by increasing the number of calibration parameters (see again table 7). These observations could also be made for other participants' results and can thus be regarded as representative. The systematic effect shown in figure 2 and its absence in figure 4 conforms well with the results presented in table 7, as does the similarity of figures 1 and 3. These results support a suggestion to include the parameters of interior orientation in the calibration procedure (see also discussion in chapter 5).

3.4 Local analysis

The results presented so far give a good overview of the potential of direct sensor orientation, and the RMS differences are surprisingly small. Thus, direct sensor orientation must be seen as a promising candidate for extracting 3D information from aerial imagery. The determination of the object space coordinates and thus the computation of the RMS differences, however, was based on multiple rays per point, not on the more realistic scenario with only two rays[4]. Also, the obtained results in image space (the σ_o values from table 5) need a closer look, because with the given results stereo plotting must be seen as problematic. A more detailed analysis aiming at quantifying the obtainable accuracy with only two rays per point and at detecting possible local systematic effects is described in this paragraph.
Firstly, we assessed individual models rather than relying on the results of multi-ray points. We computed least-squares forward intersections individually for all models which could be formed from the two test blocks (106 models for Company_1, 178 models for Company_2) and compared the resulting object space coordinates to the known values in the same way as before. Table 8 contains the results:

[4] If multiple rays are given it is more advantageous to perform an integrated sensor orientation as in phase II, since all the necessary inputs are available.

the σ_o values from table 5, the average of the RMS y-parallaxes per model, denoted $\sigma_{o,rel}$ and the RMS differences of the object space coordinates.
From the results it can be seen that σ_o from table 5 is a good approximation for the model accuracy, because in most cases σ_o and $\sigma_{o,rel}$ agree rather well. When comparing the RMS differences for the ICP between table 5 and 8 we find that in most cases the multi-ray points are more accurate by a factor of about 1.5, but some exceptions can be found.
Secondly, the estimated accuracy of the image coordinates was investigated for each model. The results shown in table 9 contain the $\sigma_{o,rel}$ values (same as in the previous table) together with the percentage of models with RMS y-parallaxes larger than 10 and 20 μm. These thresholds were chosen because in models with y-parallaxes larger than 10 μm manual stereo plotting becomes less comfortable, and it becomes cumbersome when the y-parallaxes are larger than 20 μm.
The results in table 9 suggest that while a number of model orientations from direct sensor orientation can in fact be used for stereo plotting, this is not always the case. For both data sets there is a

Table 8: Accuracy of two-ray points computed individually for each model

Participant	**Company_1 (106 models)**					**Company_2 (178 models)**				
	σ_o [μm]	$\sigma_{o,rel}$ [μm]	RMS differences at ICPs			σ_o [μm]	$\sigma_{o,rel}$ [μm]	RMS differences at ICPs		
			X [cm]	Y [cm]	Z [cm]			X [cm]	Y [cm]	Z [cm]
Applanix	-	-	-	-	-	22.2	20.2	11.3	13.9	33.1
IGI	36.7	36.6	24.7	19.3	30.4	-	-	-	-	-
ADR	55.5	57.5	38.3	24.7	48.4	32.2	22.6	16.6	20.8	17.6
FGI	27.4	26.9	16.6	11.2	15.6	13.6	13.6	6.3	5.4	12.3
GIP	22.9	27.3	11.0	9.8	13.4	14.8	16.4	8.4	6.3	10.0
ICC	25.8	27.6	12.4	13.1	14.6	13.9	15.5	7.0	5.4	11.0
inpho	27.0	27.0	14.4	11.0	13.5	14.8	15.6	6.7	6.5	10.7
LHS	44.6	43.3	21.2	18.4	14.3	-	-	-	-	-
DIIAR	22.9	27.0	12.2	12.6	14.9	12.4	15.1	5.6	4.4	11.3
IPF	24.6	27.4	16.8	11.3	14.2	19.5	16.4	12.2	12.2	17.4
IPI (tang.)	43.0	45.4	32.6	24.1	47.1	16.2	19.3	11.4	12.0	11.9
ifp	35.1	36.8	23.3	13.7	20.1	14.5	15.2	7.3	6.5	10.9

Table 9: Model accuracy in image space, based on all models of the test blocks

Participant	**Company_1 (106 models)**			**Company_2 (178 models)**		
	$\sigma_{o,rel}$ [μm]	% of models with RMS y-parallaxes		$\sigma_{o,rel}$ [μm]	% of models with RMS y-parallaxes	
		> 10 μm	> 20 μm		> 10 μm	> 20 μm
Applanix	-	-	-	20.2	89	31
IGI	36.6	86	55	-	-	-
ADR	57.5	100	86	22.6	90	34
FGI	26.9	75	35	13.6	85	13
GIP	27.3	74	36	16.4	88	15
ICC	27.6	80	37	15.5	86	12
inpho	27.0	74	34	15.6	86	12
LHS	43.3	98	78	-	-	-
DIIAR	27.0	74	33	15.1	79	13
IPF	27.4	80	37	16.4	85	15
IPI (tang.)	45.4	90	61	19.3	86	27
ifp	36.8	86	53	19.0	76	17

substantial number of models with y-parallaxes larger than 10 µm. In addition, the percentage of stereo models with y-parallaxes larger than 20 µm is rather high for the Company_1 data set. In order to further investigate this issue plots were created for all participants showing a distribution of the RMS y-parallaxes in the XY plane. As a representative example the plots for one participant (DIIAR) are presented in figures 5 for Company_1 and in figure 6 for Company_2. It can be seen that while for Company_1 two strips, namely the cross strip and a short strip in the middle of the block show distinctly larger y-parallaxes, for the Company_2 data the RMS y-parallaxes are more or less similar across the whole block.

At first sight this effect is surprising. The photogrammetric data give no evidence that an error in the image coordinates of the tie points can explain it. A possible explanation can be given when referring again to Nilsen Jr. (2002) and the GPS conditions during the Company_1 test flight. As is evident from the flight management recordings the two strips in question are the two last strips flown during the complete mission, at a considerable time interval to the other strips of the block. The images in the middle of the block could not be captured sooner due to clouds, and the cross strip was planned to be the last strip anyway. About the second half of the block was captured under unfavourable GPS constellations. The two strips discussed here were flown shortly after the PDOP had returned to a value of about 1.7. However, the time interval between the last good satellite constellation and the acquisition time of the two strips may have been too long to again reach an adequate positioning accuracy.

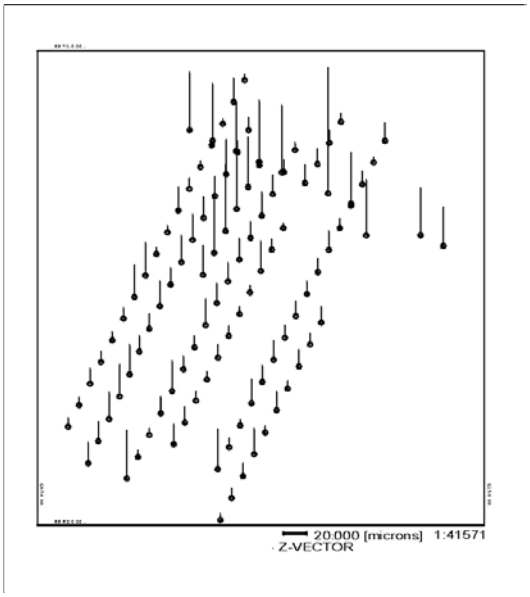

Figure 5: Remaining RMS y-parallaxes in individual stereo models, Company_1, Participant DIIAR

Figure 6: Remaining RMS y-parallaxes in individual stereo models, Company_2, Participant DIIAR

In order to test this hypothesis these two strips were discarded from the analysis procedure, and the whole process was repeated. The results for three representative participants are presented in table 10. When comparing these values to the corresponding entries in tables 8 and 9 an improvement can be seen. As was to be expected this improvement mainly concerns the results in image space, since the object space coordinates are of course not only influenced by the models of the two discarded strips. Nevertheless a small improvement is also visible in the RMS differences to the ICPs.

Table 10: Company_1 results without the two problematic strips

Participant	Company_1 88 models without the two problematic strips						
	$\sigma_{o.rel}$ [μm]	RMS differences at ICPs			$\sigma_{o.rel}$ [μm]	% of models with RMS y-parallaxes	
		X [cm]	Y [cm]	Z [cm]		> 10 μm	> 20 μm
IGI	30.1	15.9	14.6	21.7	29.4	86	49
GIP	16.0	6.9	7.9	10.2	18.0	70	26
DIIAR	16.4	7.4	10.6	11.6	17.2	68	22

In summary, it can be stated, and comes as no surprise, that the system calibration itself is more complex than one might think at first. This statement is motivated not only by the fact that direct sensor orientation is equivalent to an extrapolation, and therefore comes with all associated difficulties, but also by the fact that not all test participants have given full details of the actual procedure used for investigating the test data. While it is of course understandable that some crucial information is kept confidential, particularly in the commercial arena, this lack of information renders a conclusive interpretation of the results more difficult. Nevertheless, we feel that we were able to achieve the goals set out for phase I of the test.

4 PHASE II: INTEGRATED SENSOR ORIENTATION

Direct sensor orientation has reached a remarkable level of accuracy as reported in the previous chapter. One of the shortcomings, however, is the reduced possibility to carry out stereo plotting based on the achieved results. This fact is the main motivation for phase II of the test consisting of an integrated sensor orientation. The input data of phase II were the GPS/IMU data of the test flight, improved by system calibration parameters (results from phase I) and about twenty five image coordinates of tie points for two different subsets of the test flight images (see below). Ground control information was not provided in order to be able to investigate the influence of tie points within integrated sensor orientation, without effects stemming from ground control. It is clear that this lack of GCPs within the integrated sensor orientation also prevents the refinement of some of the system calibration parameters (e.g. GPS shift parameters, focal length; note, however, that the misalignment angles can be improved in a block configuration using only tie points) due to geometrical reasons. For a number of image coordinates included in this task corresponding ground control coordinates existed at the pilot centre which were used to check the participants' results.

4.1 Test data for phase II

When comparing direct and integrated sensor orientation, the role of IMU data changes. In both cases the IMU data serve as input for GPS/IMU pre-processing and increase the quality of the derived positions for the centre of projection during image acquisition. For direct sensor orientation the IMU data are furthermore indispensable as direct observations for the roll, pitch, and yaw angles. This is not the case anymore for integrated sensor orientation of image blocks, because these angles can also be computed from the image coordinates of the tie points. The situation again changes, if image strips rather than blocks are considered, because in this case the misalignment cannot be estimated from tie points alone.

In order to study both scenarios, we decided to investigate one block and one strip within phase II. Obviously, we wanted to create very similar conditions for Company_1 and Company_2 despite the somewhat different block geometry due to the changing weather conditions. The only possibilities for selecting (nearly) identical block and strip configurations are presented in figures 7 and 8, showing one block with five parallel strips and one cross strip (strip length between seven and ten images, fifty two images in total for Company_1, fifty three images for Company_2,) and one strip of seventeen

images. These are the test data for phase II. The forward and the side overlap were both 60 %. It can be seen in figures 7 and 8 that the flight strips of the block are not of identical length which somewhat weakens the photogrammetric block stability. However, better data were not available due to the mentioned unfavourable weather conditions. Note that due to the reduced area covered by the test data as compared to the block used in phase I, there are less ICPs available for data analysis.

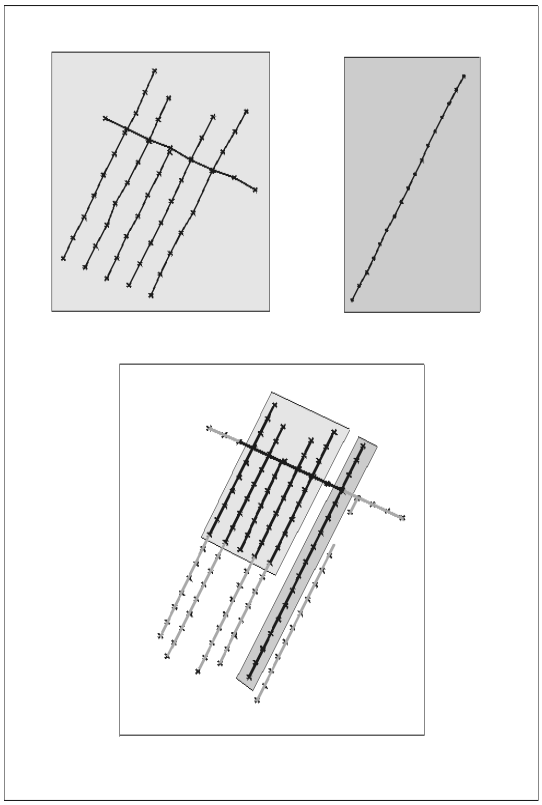

Figure 7: Company_1 test data set "Block" and "Strip", phase II,
and their location in the whole data set

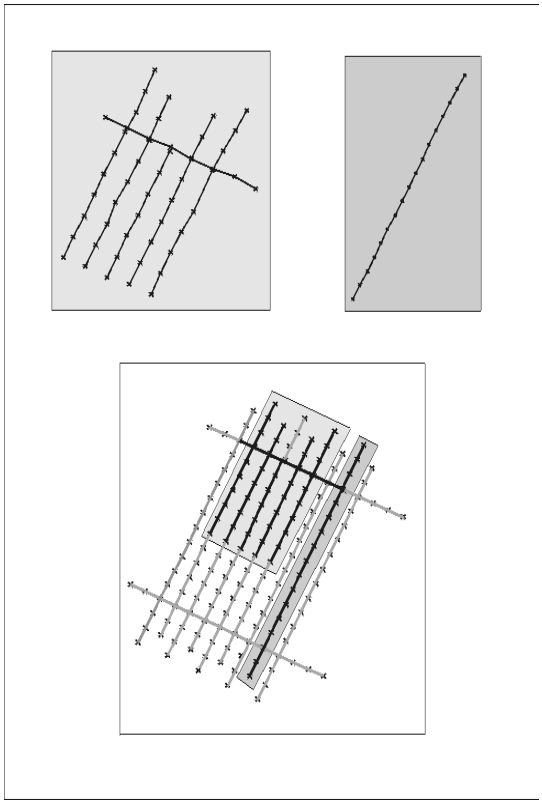

Figure 8: Company_2 test data set "Block" and "Strip", phase II,
and their location in the whole data set

4.2 Results and analysis

Eight of the twelve participants who took part in phase I sent in results for phase II (see table 2). The results are presented in the following paragraphs. The mathematical models used for the integrated sensor orientation were basically the same as the one used for system calibration. However, some changes were mentioned in the participants' reports (see table 11):

- of course, all participants performed a "1 step" procedure (see table 3, otherwise the solution would not classify as being integrated),
- most participants introduced the system calibration parameters determined in phase I as constant values, but some allowed for a refinement of at least a subset of parameters,
- some participants handled the block and the strip differently. For example they introduced additional parameters for modelling a drift of the misalignment angles in the block, but not in the strip,

- as in phase I, reliable stochastic properties of the observations, in particular those of the GPS/IMU data, were missing, and values had to be selected from experience to determine appropriate weights for the observations. Some participants also used variance-covariance estimation techniques and robust estimation. Obviously, the used weighs differed across the different participants.

Table 11: Number and type of system calibration parameters, phase II

Participant		**NO. AND TYPE OF SYSTEM CALIBRATION PARAMETER**				
		block (no. of parameters)		**strip (no. of parameters)**		**Parameters**
		const.	**unknowns**	**const.**	**unknowns**	
FGI	Company_1	$6^{1.)}$	$18^{2.)}$	$6^{1.)}$	-	1.) drpy + dXoYoZo 2.) 3 IMU offsets per strip
	Company_2	$6^{1.)}$	$18^{2.)}$	$6^{1.)}$	-	
ICC	Company_1	$6^{1.)}$	$6^{2.)} + 15^{3.)}$	$6^{1.)}$	$1^{2.)}+15^{3.)}$	1.) drpy + dXoYoZo 2.) 1 IMU drift per strip 3.) dcxpxp. 12 additional parameters
	Company_2	$6^{1.)}$	$6^{2.)} + 15^{3.)}$	$6^{1.)}$	$1^{2.)}+15^{3.)}$	
inpho	Company_1	-	$6^{1.)}$	-	$6^{1.)}$	1.) drpy + dXoYoZo 2.) dcxpyp
	Company_2	-	$6^{1.)} + 3^{2.)}$	-	$6^{1.)} + 3^{2.)}$	
LHS	Company_1	$6^{1.)}$	$3^{2.)}+18^{3.)}$	$6^{1.)}$	$3^{2.)}+18^{3.)}$	1.) drpy + dXoYoZo 2.) dcxpxp 3.) 18 additional parameters
	Company_2	$6^{1.)}$	$3^{2.)}+18^{3.)}$	$6^{1.)}$	$3^{2.)}+18^{3.)}$	
DIIAR	Company_1	$6^{1.)}$	$72^{2.)}$	$6^{1.)}$	$12^{2.)}$	1.) drpy + dXoYoZo 2.) GPS/IMU offset and shift per strip
	Company_2	$6^{1.)}$	$72^{2.)}$	$6^{1.)}$	$12^{2.)}$	
IPF	Company_1	-	$6^{1.)} + 3^{2.)} + 1^{3.)}$	-	$6^{1.)} + 3^{2.)}$	1.) drpy + dXoYoZo 2.) dcxpxp 3.) 1 additional parameter
	Company_2	-	$6^{1.)} + 3^{2.)}$	-	$6^{1.)} + 3^{2.)}$	
IPI	Company_1	$6^{1.)}$	$12^{2.)}$	$6^{1.)}$	$12^{2.)}$	1.) drpy + dXoYoZo 2.) 12 additional parameters
	Company_2	$6^{1.)}$	$12^{2.)}$	$6^{1.)}$	$12^{2.)}$	
ifp	Company_1	$5^{1.)}$	$7^{2.)}$	$5^{1.)}$	-	1.) drpy + dYo + dc 2.) drpy + 7 additional parameters 3.) dcxpyp
	Company_2	$3^{3.)}$	$10^{2.)}$	$6^{1.)}$	-	

The obtained results are presented in tables 12 and 13. In table 12 the results of the block and the strip adjustment are given, consisting of the a posteriori standard deviation of the image coordinates σ_o, and the RMS differences of the derived object space coordinates of the ICPs (nine for the block, six for the strip). Table 13 contains the RMS differences after allowing for a 3D translation of the computed cloud of tie points with respect to the ICPs (they are termed RMS* in the following to differentiate them from the RMS differences given in table 12), and the maximum differences at the ICP. The RMS* differences can be interpreted as the root mean square differences after the introduction of one GCP. The translation itself is not explicitly given, but it can be calculated from the data presented in tables 12 and 13. The translation amounts to a few cm only. As in phase I, the overall situation was somewhat heterogeneous, and conclusive interpretations for differences in the numerical results cannot always be given. Nevertheless the obtained results show some general trends of integrated sensor orientation:

- compared to direct sensor orientation, the a posteriori standard deviation of the image coordinates σ_o is greatly reduced. This finding confirms the expectations that a local refinement of the image orientation is achieved by introducing tie points. σ_o is in the same range as for the photogrammetric reference solutions (see table 1). Consequently, integrated sensor orientation does allow for stereo plotting in the same way as conventional photogrammetry.
- in planimetry the RMS differences in object space are only slightly better than in the case of direct sensor orientation (compare results in tables 12 an 13 to those in tables 5 and 6). Improvements have primarily occurred in height, in particular for Company_1. The reason only for the moderate improvements in object space is probably that the errors in the GPS/IMU values presented in phase I are primarily random in nature and thus were basically visible in image space only. This random error could be eliminated in phase II refining the image orientations through the introduction of tie points. The actual numbers should be compared with some care, however, since in phase I and II different blocks, different ICPs and partly different mathematical models were used. Most participants obtained RMS differences of 5 – 10 cm in all three coordinates, and the maximum errors are nearly all below 25 cm.
- The results for the block and the strip are rather similar, which indicates that the GPS/IMU observations are accurate enough to stabilise the photogrammetric adjustment (as was to be expected).
- For Company_1 and to some extent also for Company_2 systematic effects have been detected (compare tables 12 and 13). In particular for Company_1 these effects probably stem from the unfavourable GPS conditions. As can be seen the RMS* differences are rather close to the conventional photogrammetric accuracy.
- For some approaches additional model refinements will probably lead to further improved results.

Table 12: Results of integrated sensor orientation

Participant		**Company_1 (Block 9 XYZ_ICPs; Strip 6 XYZ_ICPs)**				**Company_2 (Block 9 XYZ_ICPs; Strip 6 XYZ_ICPs)**			
		σ_o [µm]	RMS differences at ICP			σ_o [µm]	RMS differences at ICP		
			X [cm]	Y [cm]	Z [cm]		X [cm]	Y [cm]	Z [cm]
Block	FGI	5.3	5.9	4.3	2.8	6.2	5.4	4.1	5.5
	ICC	4.0	7.9	12.1	3.9	2.6	5.5	3.1	5.5
	inpho	5.0	8.2	11.6	6.0	5.0	4.0	6.1	6.4
	LHS	5.0	11.4	13.9	9.8	5.4	2.2	2.0	10.1
	DIIAR	6.0	8.5	7.4	5.9	6.0	5.8	3.1	7.0
	IPF	4.0	4.5	3.6	3.2	5.7	3.9	3.5	8.2
	IPI (tang.)	6.9	11.4	15.5	8.3	6.2	3.2	1.1	9.5
	IPI (UTM)	7.2	11.8	14.5	8.5	6.1	3.7	3.4	13.0
	ifp	5.2	10.5	5.6	2.9	5.9	4.1	2.6	6.7
Strip	FGI	3.9	10.8	6.5	7.2	6.2	12.4	12.9	8.7
	ICC	4.3	9.3	7.2	4.4	2.5	6.9	3.4	7.2
	inpho	5.0	7.0	6.6	6.8	5.0	5.7	7.6	7.3
	LHS	3.6	7.5	5.4	2.8	3.5	5.3	4.1	13.5
	DIIAR	4.0	8.3	6.2	5.0	4.0	4.5	9.7	9.1
	IPF	3.7	6.1	3.9	5.2	5.0	5.3	3.7	9.0
	IPI (tang.)	3.8	7.7	8.5	5.9	4.2	7.1	5.1	10.4
	IPI (UTM)	3.8	7.7	6.5	5.3	4.0	4.7	4.8	14.1
	ifp	3.5	14.8	8.8	4.8	5.9	9.9	7.8	6.9

Table 13: RMS* differences and maximum differences at Independent Check Points (ICPs) in the case of integrated sensor orientation (see text for the difference between RMS and RMS* differences)

Participant		Company_1 (Block 9 XYZ_ICPs; Strip 6 XYZ_ICPs)						Company_2 (Block 9 XYZ_ICPs; Strip 6 XYZ_ICPs)					
		RMS* differences at ICP			Maximum differences at ICP			RMS* differences at ICP			Maximum differences at ICP		
		X [cm]	Y [cm]	Z [cm]	Xm [cm]	Ym [cm]	Zm [cm]	X [cm]	Y [cm]	Z [cm]	Xm [cm]	Ym [cm]	Zm [cm]
Block	FGI	2.0	3.9	2.5	8.8	8.3	5.3	2.2	4.0	4.2	8.7	7.3	9.5
	ICC	4.3	5.0	3.2	13.5	-18.5	-6.8	1.7	2.6	3.8	8.7	-5.2	10.5
	inpho	3.5	5.8	2.9	13.4	-20.2	-8.6	3.9	5.6	6.3	-5.5	10.1	14.9
	LHS	8.2	6.4	7.3	26.8	-21.3	-20.3	2.2	1.9	4.0	4.4	3.9	15.6
	DIIAR	1.1	2.8	2.5	10.5	-11.0	-8.4	2.0	3.0	2.6	8.3	-4.9	9.0
	IPF	1.5	2.6	2.7	6.7	-6.4	6.1	1.6	3.3	4.9	5.3	-5.9	16.5
	IPI (Tang.)	5.8	5.1	8.3	18.7	-23.9	-14.0	2.4	1.0	5.6	5.9	-2.4	19.6
	IPI (UTM)	5.8	5.3	8.1	19.1	-23.1	-15.0	2.4	1.0	5.8	-6.9	-5.2	24.7
	ifp	3.4	5.6	2.5	15.4	-10.1	-5.4	4.1	2.4	5.9	-7.6	4.8	15.8
Strip	FGI	5.6	3.1	4.9	16.9	10.3	15.2	12.4	11.9	7.4	21.7	-17.0	15.0
	ICC	1.6	1.6	4.3	11.5	-9.7	9.4	2.9	3.3	4.6	11.0	-5.2	10.8
	inpho	1.9	2.0	6.5	8.4	-9.1	10.5	5.5	7.1	6.9	10.4	-12.3	11.4
	LHS	3.0	3.2	2.7	10.3	-8.7	-4.5	3.1	4.1	4.4	-9.3	6.8	20.0
	DIIAR	1.9	1.1	4.0	10.3	-7.9	-6.8	3.2	3.4	6.9	-7.8	11.7	16.7
	IPF	1.3	1.6	3.9	8.2	6.1	11.4	3.6	3.4	5.8	11.3	-6.7	14.4
	IPI (Tang.)	4.5	3.3	5.3	12.2	-11.5	10.7	4.7	3.9	6.8	13.3	6.2	23.4
	IPI (UTM)	4.6	3.0	5.3	12.4	-9.2	7.8	4.7	3.8	6.7	7.3	-7.9	26.1
	Ifp	3.4	2.7	4.7	19.9	12.0	9.0	9.1	7.6	6.2	20.0	-17.1	12.2

5 CONCLUSIONS AND RECOMMENDATIONS

A very important finding is the fact that based on the obtained results **direct sensor orientation** has proven to be a serious alternative to conventional bundle adjustment. Within the test RMS differences for point determination of 5 – 10 cm in planimetry and 10 – 15 cm in height at independent check points have been obtained for multi-ray points in image scale 1:5 000. For two-ray points the RMS differences are higher by only a factor of about 1.5[5]. Obviously, the values for two-ray points are more relevant, because if multi-ray points are available, one would carry out an integrated sensor orientation. While these values are larger by a factor of 2 – 3 when compared to standard photogrammetric results, it seems to be safe to conclude that direct sensor orientation currently allows for the generation of orthoimages and point determination with less stringent accuracy requirements. Reports from practical applications demonstrate a significant decrease in time, and thus cost, for direct sensor orientation compared to conventional and GPS-photogrammetry.

[5] It should not be forgotten, however, that one of the main advantages of multi-ray points with respect to two-ray points is the improved reliability of the results.

Stereo plotting, on the other hand, is not always possible using direct sensor orientation due to the sometimes large y-parallaxes in individual models. Of course, relative orientations can be computed for each model to decrease the y-parallaxes before starting stereo plotting. This procedure is very similar to traditional stereo plotting, where the orientation was established for each model individually based on ground control points derived from a prior adjustment. While this suggestion, termed the "point interface" of photogrammetry (Colomina 2002), is certainly viable for practical applications we have not pursued it any further within the test.

Compared to direct sensor orientation the additional introduction of tie points in **integrated sensor orientation** without GCPs improves in particular the accuracy in image space, and to some extent also in object space. If a minimum of GCPs is introduced an accuracy in object space very similar to that of conventional photogrammetry is achieved, as was demonstrated with only one (simulated) GCP. Thus, as was to be expected, integrated sensor orientation overcomes the problem of remaining y-parallaxes in photogrammetric models, and allows for the determination of 3D object space information in much the same way as conventional photogrammetry. In order to model the stochastic properties of the GPS/IMU data more realistically, accuracy estimates for GPS/IMU pre-processing should be made available and should be properly introduced into integrated sensor orientation. In addition, high frequency GPS/IMU data should be made available in order to detect and eliminate possible time synchronisation problems. These requests equally hold for the calibration phase of direct sensor orientation.

Based on the obtained results, the inclusion of the interior orientation parameters in the **system calibration** is to be recommended whenever possible. If it is not feasible to use two calibration flights at signifycantly different flying heights, the calibration should be carried out at the same height (and thus the same scale) as the actual project. It should not be forgotten, however, that a refinement of the interior orientation parameters during the calibration does not necessarily mean that the camera calibration certificate contains incorrect values. It only implies, that the more general models better explain the given input data. For instance, a change in the x-direction of the principal point has nearly the same effect on the results as a constant error in the time synchronisation between the GPS/IMU sensors and the camera. The same is true for a change in the calibrated focal length and the GPS shift in Z.
The test results have been obtained immediately after calibration. Therefore, no statement can be made within this test concerning the stability of the system calibration parameters over time. It is known that the boresight misalignment can vary over time, especially when analogue photogrammetric cameras are in use. This situation is expected to improve once the new digital aerial cameras become available since they are constructed with GPS/IMU equipment in mind in the first place. Currently, it is generally recommended to carry out the system calibration before and, possibly also, after each block, at least for high accuracy work. In addition, it makes sense in integrated sensor orientation to check the system calibration parameters with the data of the actual project flight and to refine or estimate at least some of them together with the image orientation.
In order to avoid effects from non-rigorous modelling direct and integrated sensor orientation, and thus also system calibration, should be carried out in an orthogonal coordinate system, e.g. a tangential system, such as UTM (see, however, a discussion on these effects in Jacobsen 2002).

The **reliability** of the results remains a weak point of direct and integrated sensor orientation due to a lack of redundancy in absolute orientation. Systematic errors in the GPS/IMU measurements or changes in the system calibration parameters between calibration and actual flight may go unnoticed, because they cannot be detected without the introduction of GCP coordinates. Thus, it is recommended to include at least a minimum number of GCPs in the actual project area wherever possible.

Once tie points are available as is the case in integrated sensor orientation, the **additional effort and cost associated with introducing an IMU** must be separately justified, since GPS alone already pro-

vides for a geometrically stable photogrammetric block with very few GCPs. Several arguments can be made in favour of an IMU:

- The introduction of IMU improves the accuracy and reliability of GPS positions by reducing the effects of cycle slips and other errors.
- As soon as IMU data are introduced the cross strips flown in most GPS-photogrammetry applications become obsolete.
- Photogrammetric strip adjustments need a significant number of GCP if IMU observations are not available.
- Using IMU data, the necessary amount and distribution of tie points for integrated sensor orientation may be significantly reduced. It is currently an open question, how many tie points are still necessary, and where they have to be situated.
- In integrated sensor orientation it is possible to use somewhat less expensive (and less accurate) IMU, since attitude refinement is achieved through the tie points.
- Only GPS/IMU sensors allow for direct sensor orientation. If such a system has been acquired for carrying out direct sensor orientation, the IMU observations are available anyway, and should also be introduced into integrated sensor orientation.

Thus, it can be concluded that the IMU has enough technical advantages over GPS-photogrammetry to justify its use in integrated sensor orientation. As mentioned, for direct sensor orientation, the IMU is indispensable, anyway, which is probably the biggest argument in favour of the new sensor.

In summary, it is expected that direct sensor orientation will be the dominating technology for sensor orientation. Of particular relevance is a properly carried out system calibration. Integrated sensor orientation will be applied whenever very high accuracy is indispensable, and tie points are, thus, needed in order to model effects in image space using additional parameters. Also, a tighter coupling of GPS/IMU and image coordinate observations has the potential to further improve the results. Future developments in GPS and IMU sensor technology and data processing, e.g. GPS network solutions (Colomina 2002) will probably further improve the potential of direct and integrated sensor orientation.

6 ACKNOWLEDGEMENTS

The authors are grateful to the companies Applanix, IGI, Fotonor and Fjellanger Widerøe Aviation for participating in the test and for having acquired and provided the test data. We would also like to thank the Norwegian Mapping Authority Statens Kartverk, Hønefoss, for making available the measurements of the GPS reference stations and the OEEPE for their support of the project. Thanks are also due to Øystein Andersen and Barbi Nilsen Jr. from the Agricultural University of Norway who were responsible for data acquisition and handled this crucial part of the test with great wisdom and care; to Günter Seeber and his team from the Institut für Erdmessung, University of Hannover, for valuable help with the GPS data; and to Adelheid Elmhorst and Karin Kolouch from IPI who did not shy away from handling the nearly seven hundred test images in endless hours of work. Last but not least, the test would not have been possible without the enthusiastic efforts of the test participants. It was a lot of fun working together with you in this project. We hope to have fulfilled your expectations.

7 REFERENCES

ARINC 705: http://www.arinc.com/cgi-bin/store/arinc (Accessed July-3rd-2001).

Colomina I. (2002): Modern sensor orientation technologies and procedures, in: Heipke C., Jacobsen K. Wegmann H. (Eds.), Integrated Sensor Orientation, OEEPE Official Publication No. 43.

Cramer M., (2001): Genauigkeitsuntersuchungen zur GPS/INS-Integration in der Aerotriangulation, DGK-C (537), 122 p.

Forlani G., Pinto L. (2002): Integrated INS/DGPS systems: calibration and combined block adjustment, in: Heipke C., Jacobsen K., Wegmann H. (Eds.), Integrated Sensor Orientation, OEEPE Official Publication No. 43.

Habib A., Schenk T. (2002): Accuracy analysis of reconstructed points in object space from direct and indirect exterior orientation methods, in: Heipke C., Jacobsen K., Wegmann H. (Eds.), Integrated Sensor Orientation, OEEPE Official Publication No. 43.
Heipke C., Jacobsen K., Wegmann H., Andersen Ø, Nilsen B. (2002): Test goals and test set up for the OEEPE test "Integrated Sensor Orientation", in: Heipke C., Jacobsen K., Wegmann H. (Eds.), Integrated Sensor Orientation, OEEPE Official Publication No. 43.
Jacobsen K. (2002): Transformations and computation of orientation data in different coordinate systems, in: Heipke C., Jacobsen K., Wegmann H. (Eds.), Integrated Sensor Orientation, OEEPE Official Publication No. 43.
Leistner, H. (2000): Bericht über Auswertung der GPS-Daten des OEEPE Projektes: Integrated Sensor Orientation, a comparative test, Institute of Geodesy, University of Hannover, Internal report., 35 p.
Nilsen Jr. B. (2002): Test field Fredrikstad and data acquisition for the OEEPE test "Integrated Sensor Orientation", in: Heipke C., Jacobsen K., Wegmann H. (Eds.), Integrated Sensor Orientation, OEEPE Official Publication No. 43.
Ressl C. (2002): The OEEPE-test "Integrated sensor orientation" and its handling within the hybrid block-adjustment program Orient, in: Heipke C., Jacobsen K., Wegmann H. (Eds.), Integrated Sensor Orientation, OEEPE Official Publication No. 43.
Schmitz M., Wübbena G., Bagge A., Kruck E. (2002): Benefit of rigorous modelling of GPS in combined AT/GPS/IMU-bundle block adjustment, in: Heipke C., Jacobsen K., Wegmann H. (Eds.), Integrated Sensor Orientation, OEEPE Official Publication No. 43.
Schwarz K.-P. (1995): Integrated airborne navigation systems for photogrammetry, in: Fritsch D., Hobbie D. (Eds.), Photogrammetric Week ´95, Wichmann, Heidelberg, 139-153.
Schwarz K.-P., Chapman M.E., Cannon E., Gong P. (1993) : An integrated INS/GPS approach to the georeferencing of remotely sensed data, PE&RS (59) 11, 1667-1674.
Skaloud J. (1999): Problems in sensor orientation by INS/DGPS in the airborne environment, Proceedings, ISPRS Workshop "Direct versus indirect methods of sensor orientation", Barcelona, pp. 7-15.